AFCEC-CX-TY-TP-2016-0010

OPTIMIZATION AND APPLICATION OF A SMALL LACCASE (SLAC) FOR ENZYMATIC FUEL CELL DEVELOPMENT

Matthew Eby, Randi Tatum, Karen Farrington, & Heather Luckarift
Universal Technology Corporation
Dayton, OH 45432

Guinevere Strack
Oak Ridge Institute for Science & Education
Oak Ridge, TN 37831

Sofia Babanova & Plamen Atanassov
Dept. of Chemical & Biological Engineering
University of New Mexico
Albuquerque, NM 87131

Ruth Pachter
Air Force Research Laboratory
Wright-Patterson AFB, OH 45433

Lloyd Nadeau & Glenn Johnson
Air Force Research Laboratory
Tyndall AFB, FL 32403

Contract No. FA4819-11-C-0003

February 2016

AIR FORCE CIVIL ENGINEER CENTER
READINESS DIRECTORATE

■ Requirements & Acquisition Division ■ United States Air Force ■ Tyndall Air Force Base, FL 32403-5323

DISCLAIMER

Reference herein to any specific commercial product, process, or service by trade name, trademark, manufacturer, or otherwise does not constitute or imply its endorsement, recommendation, or approval by the United States Air Force. The views and opinions of authors expressed herein do not necessarily state or reflect those of the United States Air Force.

This report was prepared as an account of work sponsored by the United States Air Force. Neither the United States Air Force, nor any of its employees, makes any warranty, expressed or implied, or assumes any legal liability or responsibility for the accuracy, completeness, or usefulness of any information, apparatus, product, or process disclosed, or represents that its use would not infringe privately owned rights.

NOTICE AND SIGNATURE PAGE

AFCEC-CX-TY-TP-2016-0010 HAS BEEN REVIEWED AND IS APPROVED FOR PUBLICATION IN ACCORDANCE WITH ASSIGNED DISTRIBUTION STATEMENT.

//SIGNED//	//SIGNED//
Michael V. Henley	Joseph D. Wander, PhD
Contracting Officer Representative	Technical Advisor

REPORT DOCUMENTATION PAGE

Form Approved
OMB No. 0704-0188

PLEASE DO NOT RETURN YOUR FORM TO THE ABOVE ADDRESS.

1. REPORT DATE *(DD-MM-YYYY)*	2. REPORT TYPE	3. DATES COVERED *(From - To)*
17-02-2016	Technical Paper	3 Jan 2012 -- 30 Sept 2013

4. TITLE AND SUBTITLE

Optimization and Application of a Small Laccase (SLAC) for Enzymatic Fuel Cell Development

5a. CONTRACT NUMBER

FA4819-11-C-0003

5b. GRANT NUMBER

5c. PROGRAM ELEMENT NUMBER

6. AUTHOR(S)

Matthew Eby (1), Guinevere Strack (2), Lloyd Nadeau (3), Randi Tatum (1), Karen Farrington (1) Sofia Babanova (4), Plamen Atanassov (4), Ruth Pachter (5), Glenn Johnson (3), Heather Luckarift (1)

5d. PROJECT NUMBER

5e. TASK NUMBER

5f. WORK UNIT NUMBER

X13SY002

7. PERFORMING ORGANIZATION NAME(S) AND ADDRESS(ES)

(1) Universal Technology Corporation, Dayton, OH 45432, (2) ORISE, Oak Ridge, TN 37831, (3) AFRL/RXQ, Tyndall AFB, FL 32403, (4) University of New Mexico, Albuquerque, NM (5) AFRL/RXP, Wright Patterson AFB, Dayton, OH

8. PERFORMING ORGANIZATION REPORT NUMBER

9. SPONSORING/MONITORING AGENCY NAME(S) AND ADDRESS(ES)

Air Force Civil Engineer Center
Readiness Directorate
Requirements and Acquisition Division
139 Barnes Drive, Suite 2
Tyndall Air Force Base, FL 32403-5323

10. SPONSOR/MONITOR'S ACRONYM(S)

AFCEC/CXA

11. SPONSOR/MONITOR'S REPORT NUMBER(S)

AFCEC-CX-TY-TP-2016-0010

12. DISTRIBUTION/AVAILABILITY STATEMENT

Distribution A: Approved for public release; distribution unlimited. AFCEC-201916; 14 June 2019.

13. SUPPLEMENTARY NOTES

Document contains color images.

14. ABSTRACT

This report describes technical effort in the development of enzymatic fuel cells for power generation, specifically in optimization of a 'small laccase' (SLAC) from *Streptomyces coelicolor*. The work includes an optimized method for purification of homogeneous SLAC by recombinant expression in *Escherichia coli*. The improved expression and purification method provides a protein preparation that consists of one form of the holoenzyme with more consistent oxidative and electrochemical properties.

Validation of theoretical observation was also undertaken by experimental investigation to determine if specific mutations at the T1 Cu site would increase the redox potential of SLAC. Increasing the redox potential in turn increases the half-cell potential, and hence overall productivity, of an enzyme fuel cell.

15. SUBJECT TERMS

Small laccase, SLAC, Streptomyces coelicolor, Enzyme Fuel Cell, Recombinant expression, Electrochemistry, T1 copper

16. SECURITY CLASSIFICATION OF:			17. LIMITATION OF ABSTRACT	18. NUMBER OF PAGES	19a. NAME OF RESPONSIBLE PERSON
a. REPORT	b. ABSTRACT	c. THIS PAGE			Michael V. Henley
U	U	U	SAR	39	19b. TELEPHONE NUMBER *(Include area code)*

TABLE OF CONTENTS

LIST OF FIGURES

Page

LIST OF TABLES

Page

1. SUMMARY

This report summarizes the objectives, progress, and outcome of technical effort performed by Universal Technology Corporation (UTC) under prime contract FA4819-11-C-0003, for the period 3 January 2012–31 September 2013. The primary goal of the effort was to advance the utility of enzymatic fuel cells (EFCs) for power generation. The work describes how understanding fundamental biological and biophysical phenomena can be used to develop rational biotechnology solutions for Air Force requirements. Particular emphasis throughout is the integration of catalytically active biomolecules with support matrices and the utilization of these hybrid materials for development of EFCs. This report is further to technical report AFRL-RX-TY-TR-2012-0039 (DTIC # ADB384217).

This report summarizes research and development of EFCs, specifically in optimization of a 'small laccase' (SLAC) from *Streptomyces coelicolor* as a cathodic catalyst. The work includes an optimized method for purification of homogeneous SLAC that improves on current published methods. Previous recombinant expression and purification of SLAC has resulted in the isolation of various forms of the enzyme that differ in amino acid length and polymeric structure, caused by post-translational modifications of the protein. Recombinant expression systems were developed whereby SLAC was truncated at both termini to mirror the native enzyme. Codon usage was optimized to allow recombinant expression in *Escherichia coli*. The improved expression and purification method provides a protein preparation that consists of one form of the holoenzyme with more-consistent oxidative and electrochemical properties.

SLAC has a distinctive blue color that arises from very specific ligand-to-metal coordination within the protein structure. In copper-containing proteins, the interaction between the axial ligand and the copper (Cu) is dependent on several factors, including the identity of the ligand, the distance between the ligand and the Cu, the local protein environment, the protein structure, and the pH of the surrounding solution. In SLAC, the interaction with the type 1 (T1) Cu is via a weak axial methionine (M) ligand, but computational results suggested that the changes in the axial amino acid of the T1 Cu site would strongly influence the redox potential. Validation of the theoretical observation was undertaken by experimental investigation to determine the effect of specific mutations on the redox potential of the T1 Cu site. The overarching goal of increasing the redox potential is to increase the half-cell potential, and hence overall productivity, of an EFC. The electromotive force that drives the performance of an EFC is dictated by the inherent thermodynamic potential of the enzyme's redox center. Thus, increasing the redox potential of multicopper oxidases by engineering the enzyme would have a significant impact on EFC technological development.

2. INTRODUCTION

Enzymatic fuel cells (EFCs) provide a technology solution to small, lightweight, sustainable sources of power that use simple renewable fuels. EFCs have two primary operational advantages over alternative technologies for generating power from organic substrates: high conversion efficiency and operation at ambient temperatures. Conventional fuel cells use inorganic catalysts and precious metals in anodic and cathodic half-reactions separated by a barrier that selectively allows passage of positively charged ions. EFCs follow the same basic principle but redox enzymes catalyze the electrochemical processes. EFCs use specific enzyme(s) that, when electrically contacted with an electrode, will oxidize energy-rich abundant organic raw materials such as alcohols, organic acids, or sugars in the anode. In the cathode, substrates such as molecular oxygen (O_2) or hydrogen peroxide (H_2O_2) are reduced. In combination with the anodic reaction, this process generates electrical power (voltage and current) [1].

Although enzymes have been tailored by Nature to serve as selective biocatalysts, coupling that inherent activity with a functional surface (such as an electrode) can be technically challenging. To integrate biocatalysis and electrochemistry, a mechanism of direct bioelectrocatalysis is preferable, in which direct electron transfer (DET) is achieved between the enzyme catalytic center and the conductive support. Several factors, however, influence the electron transfer kinetics of DET, including the distance between the enzyme redox center and the electrode, the difference between the potential of the electron donor and the electron acceptor, and the reorganization energy of the protein and the surrounding solvent molecules [2]. It is important, therefore, to evaluate various electrode designs, including electrode material and enzyme tethering methods, to optimize the electron transfer kinetics. Previous reports have demonstrated that the efficiency of DET is enhanced between carbon nanostructures, specifically carbon nanotubes (CNTs) and redox enzymes [3–6]. Although effective DET on CNTs has been readily demonstrated at the laboratory scale, the further application of this technology requires simple, easy-to-fabricate, scalable architectures and rational design. The current most feasible concept is to press CNTs into a planar sheet, known as buckypaper (BP) [4–8]. BP is held together via physical forces (namely van der Waals attraction) and interlocking CNTs, and provides high conductivity that negates the need for additional current collectors. However, a robust tethering method to provide an optimal electronic connection is required between the enzyme redox center and the conductive support to stabilize the biocatalyst on the CNT surface. One such tethering method employs a heterobifunctional cross-linker, 1-pyrenebutanoic acid, succinimidyl ester (PBSE). In prior technical efforts, PBSE was used to immobilize multicopper oxidases (MCOs) on nanostructured carbon electrodes to produce enzyme-modified cathodes with high current density [3, 4, 8–10].

2.1. Cathodic Catalysts: MCOs

The industrial and technological applications of MCOs include the oxidation of industrial substances [11, 12], and the development of EFC cathodes for use in environmental settings [8] or implantable devices [13–17]. The immobilization of biocatalysts on nanostructured carbon

architectures can produce electrodes used to generate power in EFC. Fuel is oxidized (or reduced) on the surface of the electrode with concomitant transfer of electrons to (or from) the electrode via a tunneling event. MCOs are biocatalysts that reduce oxygen in a four-electron–four-proton reaction in the presence of an electron donor [18]. The electron donor reduces the type 1 (T1) Cu center from Cu(II) to Cu(I). The T1 complex is conserved in all MCOs and involves three amino acid residues—two histidine (H) and one cysteine (C) [19]. The T1 Cu center is reduced by the electron donor, and the electron is then transferred to three other Cu centers, classified as type 2 (T2) and type 3 (T3), via an intramolecular transfer mechanism involving the Cu–C bond [18, 20, 21]. The reduction of diatomic oxygen takes place at the T2/T3 Cu cluster and is often considered to be the rate-limiting step in the electron transfer pathway. The application of MCOs as oxygen reduction catalysts to generate cathodic current is a highly desirable technology given the relatively positive onset potential compared to carbon alone. Several MCOs have been applied as oxygen reduction catalysts, including bilirubin oxidase and phenol oxidase; however, the operating conditions are limited to acidic, Cl^--free environments. As an MCO, SLAC reduces oxygen under neutral conditions in both mediated and DET bioelectronic systems [22].

2.1.1. SLAC

Identification and isolation of SLAC from the soil bacterium *Streptomyces coelicolor* A3(2) was first reported by Machczynski, *et al*. [23]. The enzyme is unique in the family of laccases and four-copper oxidases, in that it is constructed of two domains rather than three, and exhibits an exceptionally high phenol oxidase activity at pH 9.4 against 2,6-dimethoxyphenol (DMP). In addition, SLAC is reported to be resistant to inhibition by chloride ions in both biochemical and electrochemical settings [23, 24]. High relative activity at neutral pH and resistance to chloride inhibition render SLAC suitable for various applications, such as EFCs and implantable devices that operate in physiological conditions [13–16].

Diversifying the operating scenarios requires that the interaction of each MCO with the electrode surface be understood to allow selecting the best available enzyme to thrive in the target conditions. Whereas SLAC retains the aforementioned desirable aspects, the open circuit potential (OCP) of SLAC-coated CNTs is ~0.15 V lower than an alternative MCO in identical conditions [23–25]. Structural and bioelectrochemical aspects of SLAC that lead to its unique kinetics and redox potential compared to other MCOs are central features of this study.

A desirable attribute of SLAC lies in its bacterial origin: the gene can be amplified, cloned, expressed, and ultimately purified from *Escherichia coli*. The mass of SLAC was estimated by mass spectrometry to be 32 kDa, but this is significantly lower than expected from the sequence (36.9 kDa). *N*- and *C*-terminal sequencing analysis determined that the purified protein loses a significant portion of the *N*-terminus and *C*-terminus (34–42 amino acids, and 7 amino acids respectively). In addition, the enzyme in solution is a highly thermostable dimer. Gel filtration chromatography confirmed the mass of the holoenzyme to be 69 ± 8 kDa and a protein band representing the dimer migrated intact after heating the protein preparation and measuring the size by SDS–PAGE (sodium dodecyl sulfate–polyacrylamide gel electrophoresis). In a gel activity stain with 3,4-dihydroxyphenylalanine, activity was retained in the dimer protein band,

yet the monomer protein band was inactive [12]. Subsequent studies on SLAC led to conflicting measurements of the monomer size and multimerization of the protein. In a 2008 study by Dubé, *et al*., for example, the SLAC gene was cloned into a *Streptomyces* expression-secretion vector and purified from the native strain with a monomer molecular weight of 32 kDa [12]. The enzyme exhibited optimal catalytic efficiency for DMP oxidation at pH 9 and appreciable activity was retained at 70 °C. The results were consistent with those reported by Machczynski, *et al*. [23]. In contrast, the Dubé study did not report a dimer band in SDS–PAGE gels and activity staining with 2,2'-azino-bis(3-ethylbenzthiazoline-6-sulfonic acid) confirmed activity of the preparation, but the assay was completed on a native PAGE gel and the size of the active band was not determined. In contrast, recombinant expression of SLAC in *Aspergillus oryzae* resulted in a truncated protein with activity observed only in the trimeric form [11]. The trimeric structure of SLAC is stabilized by unique loops connecting neighboring protein chains. SLAC possesses several unique structural characteristics; for example, the Cu centers are located near the surface of the central part of the assembled trimer, making the substrate binding site more accessible to solvent than similar proteins. In fact, SLAC lacks an α-helical region above the T1 complex, which exposes an H residue (H293) on the surface of the protein (Figure 1). The shallow substrate binding pocket can interact with smaller substrates via van der Waals forces, whereas larger substrates likely interact with more than one protein chain.

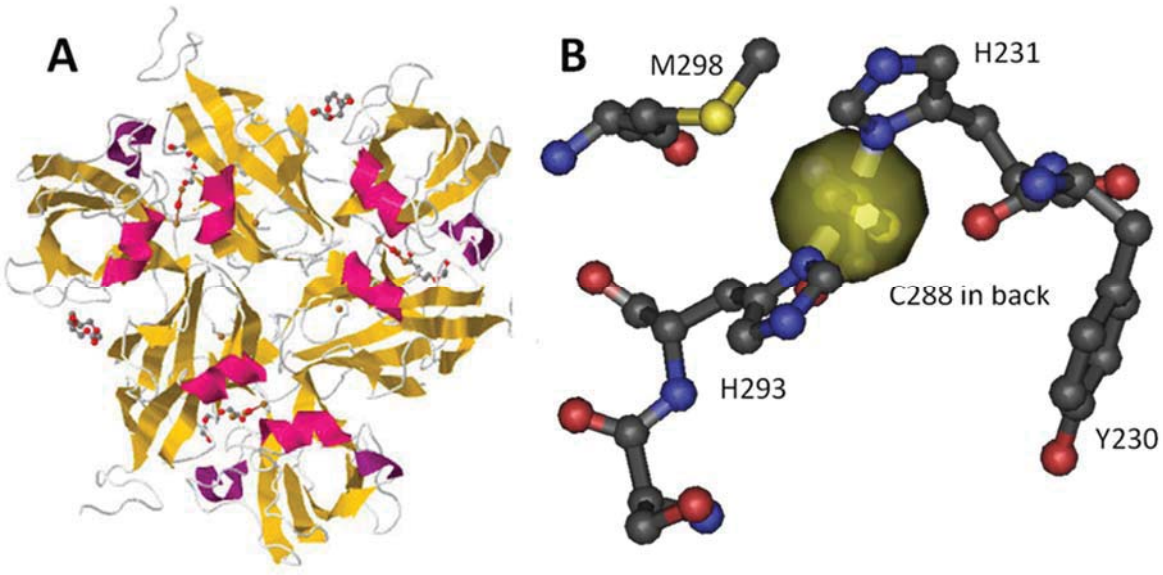

Figure 1: Representation of SLAC in the Assembled Trimeric Form (A) and the Amino Acids Associated with T1 Catalytic Copper Site (B)

SLAC has a distinctive blue color that arises from the ligand-to-metal charge transfer (LMCT) between cysteine and Cu and particular overlaps between the Cu–C orbitals [11, 23, 26–31]. The *d–d* transition energies are relatively low and result in an absorbance band in the near infrared (IR) region of the visible spectrum. In Cu-containing proteins, the interaction between the axial ligand and the Cu is dependent on several factors, including the identity of the ligand, the

distance between the ligand and the Cu, the local protein environment, the protein structure, and the pH of the surrounding solution. In SLAC, interaction with the T1 Cu is via a weak axial methionine (M) ligand, M298 (Figure 1). Engineering of the T1 redox center can be facilitated by computational investigation [19]. Reduction potentials of the azurin T1 Cu center, for example, were examined by replacing the axial ligand and several other residues in the redox center [32]. In spite of the comprehensive nature of the study, a clear pattern that could be applied toward the systematic tuning of the T1 Cu site was not established due to indirect effects contributed by protein conformations.

Results from various simulations determined that the axial amino acid of the T1 Cu site (M298 in SLAC) strongly influences the redox potential [26, 32–34]. In addition, prior calculations demonstrated reasonable suppositions of the effect of altered redox potential through variation of neighboring residues; namely, the proximate M198 and T232 (Figure 2). Calculated electron affinities based on the crystal structure of SLAC postulated that mutations of M198 and T232 could potentially increase the redox potential of the T1 Cu site in SLAC. Molecular dynamic trajectory analyses demonstrated a larger expected T1 Cu potential when M198 and T232 were changed to valine (V) and leucine (L), respectively.

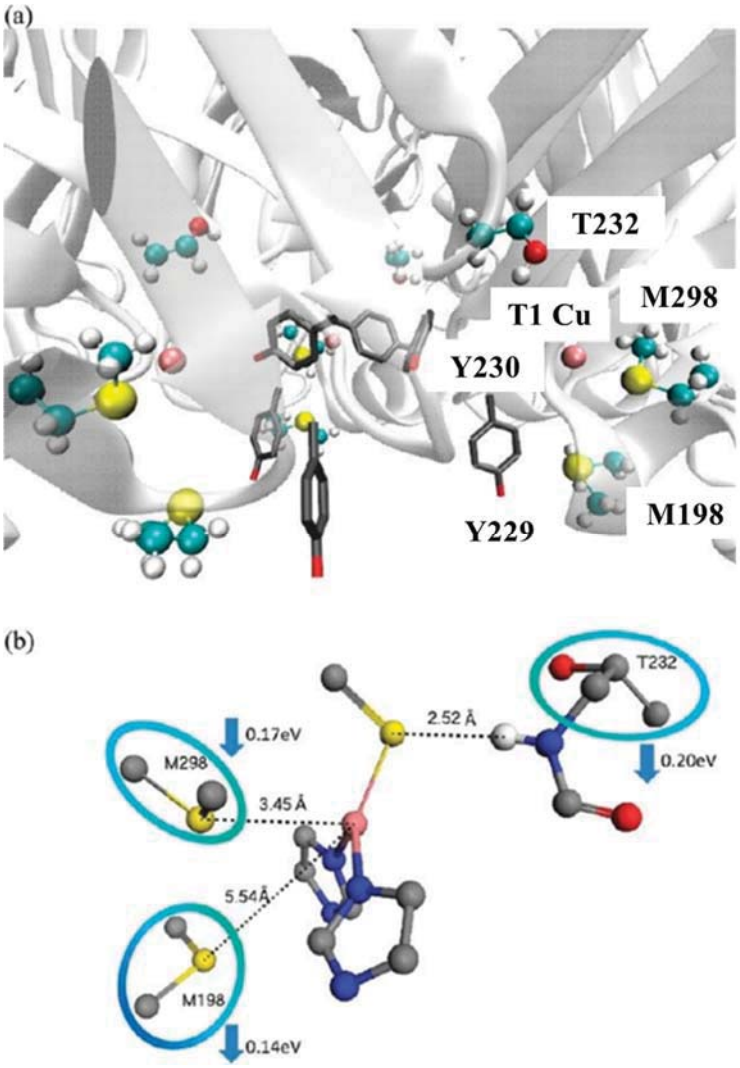

Figure 2: Hydrophobic Binding Pocket in SLAC and Suggested Amino Acids for Variation Based on the X-ray Crystal Structure for Various Model Compounds of SLAC (19).

A review of axial ligands in several MCOs revealed that the presence of a phenylalanine (F) residue in the axial ligand position (such as in laccase from *Trametes versicolor*), correlated with a higher redox potential than other MCOs, namely a Cu-dependent laccase of *Bacillus subtilis* (CotA), laccase from *Escherichia coli* (CueO), and SLAC, which all have M axial ligands. Therefore, the replacement of the M298 axial ligand with F was proposed. In addition to the axial ligand, other proximal amino acid residues in the T1 binding pocket were considered. Removal of the hydrogen bond between T232 and C288 (a Cu-binding C residue), for example, could increase the electron density of the T1 Cu complex and/or enhance the mobility of the protein backbone. Herein, we replaced the M298 axial ligand with a hydrophobic F residue (M298F) and investigated the resulting biocatalytic, optical and electrochemical changes. We

also investigated a double mutant, M298F–T232V, in which T232 was replaced with a small, hydrophobic V residue.

Lastly, theoretical calculations suggested that the blue Cu SLAC can be transformed into a ‘green’ Cu protein by replacing the relatively weak axial ligand with a stronger axial ligand or decreasing the distance between the ligand and the reactive T1 Cu atom. Validation of the theoretical observations was undertaken by experimental investigation to determine if mutations at these residues would increase the redox potential of the SLAC T1 Cu site.

3. METHODS, ASSUMPTIONS, AND PROCEDURES

3.1. Amino Acid Abbreviations

For clarity, a summary of amino acid abbreviations used throughout is summarized in Table 1.

Table 1. Amino Acid Abbreviations

AMINO ACID	ABBREVIATIONS	
	3-LETTER	1-LETTER
Cysteine	Cys	C
Histidine	His	H
Leucine	Leu	L
Methionine	Met	M
Phenylalanine	Phe	F
Threonine	Thr	T
Tyrosine	Tyr	Y
Valine	Val	V

3.2. Preparation of SLAC Variants

The SLAC gene used in this study was synthesized *de novo* by GenScript (Piscataway, NJ). The gene was engineered by encoding an M and residues 42–317 of the full-length protein sequence (GenBank accession # CAB45586) and adding stop codons at the 3′ terminus. Codon optimization for *E. coli* was also completed by GenScript using a proprietary OptimumGene™ Gene Design algorithm. This wild type (WT) gene variant was cloned into pET15b (Novagen, EMD Millipore, Billerica, MA) at the *Nde*I and *Bam*HI recognition sequences. Mutant genes with axial ligand replacements were synthesized in the same manner as the WT with the following changes: a single mutant was created in which M298 was replaced by an F and a double mutant was created by replacing T232 of the M298F mutation by a V (M298F–T232V). Proximal residue replacements included five purified and expressed variants—M198L, T232V, T232F, M198L–T232V, and M198L–T232F. Y229C, a variant in which a surface tyrosine (Y) residue was replaced by a C residue, was also synthesized. Truncated mutations of the SLAC gene were synthesized *de novo* by GenScript as above.

Growth media was manufactured by Difco (Becton, Dickinson and Company, Franklin Lakes, NJ) and all other chemicals were purchased from Sigma–Aldrich (St. Louis, MO) unless otherwise noted. *E. coli* was cultured in double-strength yeast tryptone broth supplemented with chloramphenicol (0.034 g L^{-1}) and ampicillin (0.1 g L^{-1}). All cultures were grown at 37 °C with shaking unless otherwise noted. An overnight culture (15 mL) of *E. coli* BL21 (DE3) pLysS Star (Invitrogen, Thermo Fisher Scientific, Waltham, MA) was transformed with each plasmid in a separate 1.5-L culture. When the optical density (OD; 600nm) reached ~1.5, 0.8 mM of isopropyl β-D-1-thiogalactopyranoside was added and the temperature was decreased to 25 °C. After 16 h of incubation, the cells were pelleted and resuspended in sodium phosphate buffer (10 mM, pH 7.2) (PhB) with 1 mM $CuSO_4$, DNase (0.30 g), RNase (0.03 g), and 1 mL of protease inhibitor cocktail. Cell-free extracts were made by passing cell suspensions twice through a French press

at 16 kpsi cell pressure (SLM Instruments, Inc. Urbana, IL). Cell-free extracts were centrifuged at 15,000 rpm for 30 min using a Sorvall SS-34 rotor and RC 5B plus centrifuge (Thermo Fisher Scientific) and supernatant was collected and dialyzed against three exchanges of PhB (2 L), containing 1 mM $CuSO_4$ (step 1), followed by 1 mM ethylenediaminetetra-acetic acid (EDTA; step 2), and finally with PhB only. Lysate volumes were reduced in an Amicon Ultra 15 spin filter concentrator (10k MWCO, Amicon Ultra 15, Millipore EMD, Billerica, MA) according to the manufacturer's instructions. Concentrated lysates were diluted (1:1) with 20 mM potassium phosphate buffer, 500 mM NaCl, and 20 mM imidazole at pH 7.2 (equilibration buffer; EqB) and loaded onto a cobalt–nitrilotriacetic acid affinity column (GE Healthcare, Piscataway, NJ). All column chromatography was completed on a Pharmacia Biotech HPLC System (Uppsala, Sweden). Polyhistidine (His-tag) column purification was completed according to the manufacturer's instruction. Fractions containing SLAC variants were eluted with EqB containing 500 mM imidazole. Fractions were concentrated using spin filter concentrators as described above and repeatedly diluted with 10 mM sodium phosphate (pH 7.5) and concentrated until the imidazole and NaCl concentrations were below 50 μM. Final concentration was completed using spin filter concentrators until the protein concentration was greater than 10 mg mL^{-1}. The product was stored at –20 °C until further use.

3.2.1. SLAC Activity Assays

Syringaldazine assays were performed on a Synergy 4 Microplate Reader (Biotek Inc., Winooski, VT). The assay was completed in 96-well microtiter plates with 3–10 mg mL^{-1} SLAC using a standard protocol (Sigma–Aldrich, SPSYRI01) and a total reaction volume of 0.3 mL. Changes in optical density were monitored at 530 nm. Activity assays containing DMP were completed with the same protocol using 5 mM DMP as the substrate.

3.2.2. Spectrophotometric Characterization of SLAC

SLAC variant solution concentrations and purity were determined spectrophotometrically at 590 nm (ε = 4400 M^{-1} cm^{-1}) and at 280 nm (ε = 1000 M^{-1} cm^{-1}). The absorbance value at 590 nm is indicative of the T1 Cu center and was used to determine the concentration of active SLAC monomer. Total protein concentration was determined at 280 nm and purity was determined by the ratio of the two concentrations (C_{590nm}/C_{280nm}). pH titration curves were established as follows: purified SLAC solutions (M298F, 8.5 mg mL^{-1}; M298F–T232V, 7.0 mg mL^{-1}) were added to 0.1 M buffer (phosphate/citrate at 3<pH<8; Tris at pH 9) and allowed to equilibrate for 16 h at 4 °C. An aliquot of SLAC suspension (0.1 mL) was loaded into a 0.1 mL quartz cuvette (path length = 0.1 cm) and placed in a Jasco EMC-759 Ultra Microcell Holder (Jasco Products Company, Oklahoma City, OK) and scanned from 700 nm to 340 nm using a Jasco V-670 spectrophotometer and associated software.

3.3. PBSE Modification of BP Electrodes

Circular discs (A = 0.13 cm^2) of various CNT BP materials consisting of: 1) BP prepared from 100% multiwalled CNTs (MWBP), 2) BP prepared from single-walled CNTs (SWBPs), and 3) BP prepared from 100% oxidized or "functionalized" multiwalled CNTs (MWBP-F) (Buckeye Composites; NanoTechLabs, Kettering, OH). Electrodes were conditioned in PBSE (10 mM in dimethylsulfoxide [DMSO]) for 1 h at room temperature, blotted to remove excess PBSE/DMSO

and rinsed in potassium phosphate buffer (10 mM, pH 7.0) (10). After rinsing in buffer, the BP electrodes were immediately incubated with SLAC (2 mg mL^{-1} (based on the absorbance at 590 nm)) for 2 h at room temperature. Electrodes were used immediately or stored in buffer used for electrochemical measurements at 22 °C.

3.4. Electrochemical Analysis

Enzyme-functionalized BP circular electrodes were placed on a glassy carbon disk electrode (Metrohm USA, Riverview, FL) and secured with a Teflon® cap fabricated to fit. A reference electrode Ag/AgCl (Metrohm) and a platinum wire counter electrode (Metrohm) completed the three-electrode system. The electrodes were placed in an electrochemical chamber (50 mL European five-neck flask; Ace Glass, Vineland, NJ). Electrochemical characterizations were carried out using a potentiostat (Versastat 3, Princeton Applied Research; Oak Ridge, TN) and the associated software. All potentials were reported vs. Ag/AgCl throughout. All electrochemical characterizations were performed in oxygen-saturated electrolyte. OCP, cyclic voltammetry (CV), and steady-state current densities were obtained by using a freshly prepared electrode for each analysis set. OCP measurements were performed by allowing the recorded voltage to stabilize for 30 min. CV scan rates were 5 mV/sec. Current densities were obtained by applying 0.15 V for 10 min intervals. Electrochemical activity measurements were performed in 0.1 M McIlvain's buffer for pH values 4.3, 5, 6, 7, and 8 in the presence of bubbling O_2. OCP, CV, and steady-state current density were obtained using a fresh electrode for each pH value. CVs were used to determine onset potentials and half-wave potentials. Onset potentials were defined as the voltage value corresponding to a change in current equal to three times the standard deviation of the average current at 0.4 V. Half-wave potentials (or the inflection point in a sigmoidal function) were determined by taking the second derivative of the cathodic sweep as zero.

3.5. Scanning Electron Microscopy (SEM)

BP samples were sputter-coated with gold for 30 s using a Desk-V gold sputter (Denton Vacuum, LLC, Moorestown, NJ) and imaged with a S-2600N SEM (Hitachi High Technologies, Inc., Pleasanton, CA) at an accelerating voltage of 25 kV.

3.6. Characterization of Y229C SLAC on Gold Nanoparticles (AuNPs)

The orientation of Y229C SLAC on gold was verified with SLAC–AuNP suspensions. SLAC proteins were conjugated to AuNPs (20 nm; ~1 A_{520} units mL^{-1}) with and without the addition of dithiothreitol (DTT) [35]. WT SLAC and Y229C (60 μM) were incubated with 10 mM DTT in 10 mM phosphate buffer (pH 8.0) at room temperature for 30 minutes prior to the addition of AuNPs (1% v/v final concentration). The suspensions were subjected to gel electrophoresis to determine the extent of interaction between SLAC and the AuNPs. The SLAC–AuNP solutions were incubated for 10 min at room temperature, then mixed with glycerol (5 % v/v final concentration), and loaded into agarose gel (0.8%; 22.5 mM Tris–borate, 1 mM EDTA; pH 8.3). The gels were run at 75 V for 1 h.

3.6.1. UV-Vis Spectral Characterization of Y229C SLAC-AuNP Suspension

SLAC proteins (WT and Y229C; 60 μM) were incubated with 1 mM DTT in 10 mM phosphate buffer (pH 8.0) for 30 min at room temperature before the addition of AuNPs (20% v/v final concentration). The SLAC–AuNP solutions were incubated for 2 h at 4 °C and allowed to warm to room temperature. Absorbance measurements were performed using a Cary 3E UV–Vis spectrophotometer to characterize absorbance peak changes associated with surface plasmon resonance (SPR).

4. RESULTS AND DISCUSSION

MCOs comprise a large family of enzymes, and many MCOs (e.g., laccase and bilirubin oxidase) have been applied as oxygen reduction catalysts on various electrode architectures. Although the OCP of such systems can approach optimal thermodynamic values, the operating conditions are limited to acidic pH and Cl^--free environments. SLAC, by comparison, reduces oxygen in the neutral to basic pH range and can tolerate Cl^- environments. The OCP of SLAC on CNT-based electrodes, however, is ~0.150 V lower than with laccase as a catalyst. Therefore, it is prudent to explore the structural components of the catalytic center and modify the redox potential of SLAC for application as a fuel cell catalyst. Recent molecular dynamic simulations characterized structure–function relationships between SLAC and other MCOs, and identified potential mutations that would alter the T1 Cu redox potential [19]. Herein, variant forms of SLAC were purified from an *E. coli* recombinant expression system and characterized based on electrochemical properties to validate the theoretical models.

4.1. Purification of SLAC

The SLAC gene was expressed in a Novagen® pET system vector with the 5′ and 3′ ends of the gene truncated to eliminate post-translational modifications that occur after enzyme synthesis. Codon usage of the gene was optimized for enhanced expression in *E. coli* and a His-tag affinity system was adopted for ease of purification. The purification method provided consistent preparations of active SLAC at ~70% purity (Appendix A). Direct bioelectrocatalysis of the purified WT SLAC on BP electrodes was confirmed via CV in oxygen-saturated electrolyte (Figure 3).

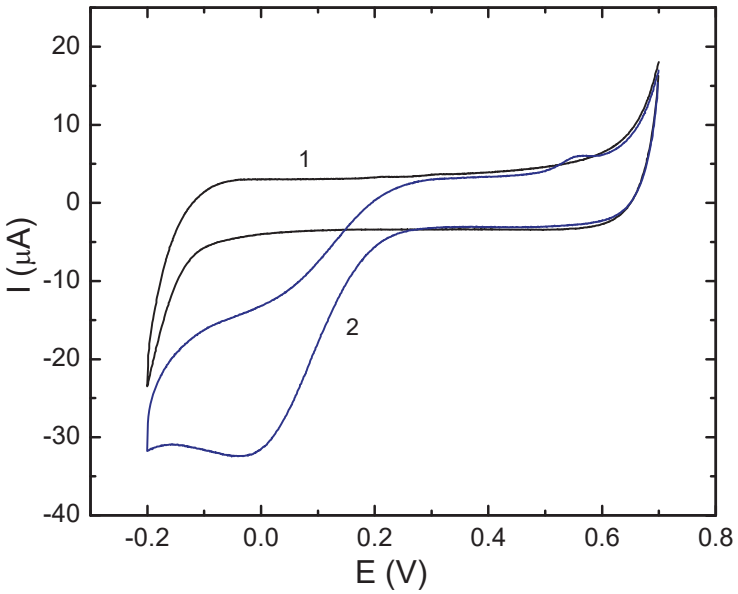

Figure 3: Cyclic Voltammograms of BP (1) and SLAC-Modified BP (2) in Oxygen-Saturated Electrolyte, pH 7.0

The OCP of the SLAC–BP electrode was determined to be 0.395 V ± 0.007; n=4. The cathodic wave beginning at ~0.250 V is indicative of a catalytic process; this process is not observed in the absence of the biocatalyst. The small peak present in the cathodic sweep at ~0 V is due to the reduction of surface-confined oxygen. Potential regions > 0 V indicate catalytic processes limited by mass transport. The half-wave potential was calculated using the cathodic sweep and was determined to be 0.096 V ± 0.01; n=3.

4.2. Analysis and Characterization of SLAC Variants

All SLAC variants were purified as a single peak from affinity chromatography and purity varied between 50–70% (Appendix A). After dialysis with Cu^{+}, all variants exhibited catalytic activity for oxidation of syringaldazine and DMP. All variants were shown to contain a T1 Cu site, evidenced as absorbance maxima at 590 nm. A comparison of UV–Vis spectra obtained for each SLAC variant confirmed that the blue appearance of each protein preparation corresponded to an absorbance band at ~600 nm associated with T1 coordination sphere and correlates with the low energy region or the $p\pi$(C)-to-Cu^{2+} LMCT band (Figure 4) [26–28, 30, 31, 34, 36]. An additional absorbance band at ~400 nm associated with the $p\sigma$(C)-to-Cu^{2+} LMCT was not observed for any of the variants. This result suggests that amino acid replacements did not contribute to distortions of the T1 coordination sphere associated with the coupled distortion model.

Enzyme-catalyzed oxygen reduction reactions (ORRs) typically reach an optimal catalytic turnover rate, k_{cat}, in acidic conditions due to the demand for four protons during the four-electron reduction process. When DMP is the electron donor, SLAC exhibits an optimal k_{cat} at pH ~8.0 and a low Michaelis–Menten constant, K_M, in basic conditions [23]. Hence, catalytic efficiency, k_{cat}/K_M, is highest near pH 9.0. This atypical catalytic performance is likely due to the hydrophobicity of the T1 binding cleft, the pK_a of DMP and binding pocket Y residues.

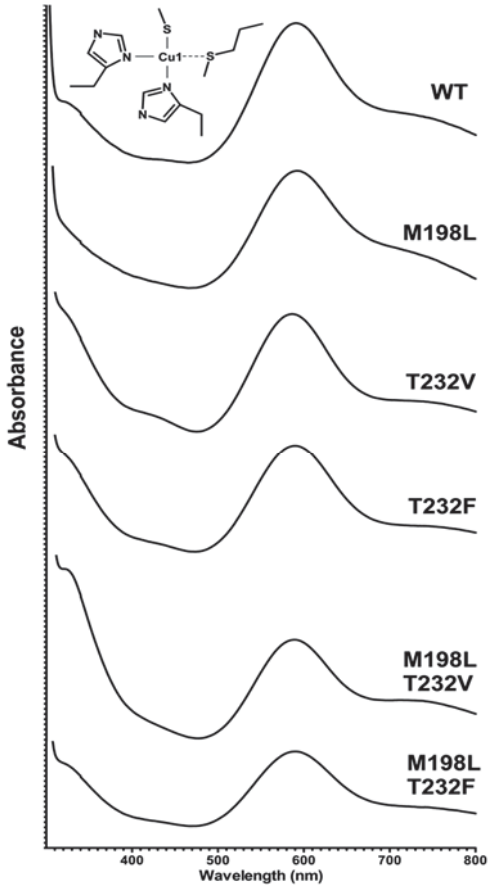

Figure 4: Absorbance Spectra of SLAC Variants

Note: The absorbance band at 590 nm is associated with the LMCT band resulting from the Cu–C bond.

The WT k_{cat} was determined experimentally (at pH ~7.7) and is in good agreement with previous work [12].Optimal activity for T232V and T232F shifted toward the acidic direction and was determined to take place at pH ~7.0 and 6.7, respectively (Table 2).

Table 2: Electrochemical and Biochemical Characterization of SLAC Variants

	OCP (V)[a]	I_{0V} (μA) [a, b]	Onset Potential (V) [a]	$E_{½}$ (V) [a]	pH optimum	
					I_{ss} [c]	k_{cat} [d]
WT	0.403 ± 0.001	–35.1 ± 3.6	0.307 ± 0.007	0.096 ±0.010	5.6	7.7
T232F	0.392 ± 0.009	–9.76 ± 0.2	0.358 ± 0.001	ND[e]	5.8	7.0
T232V	0.390 ± 0.008	–30.61 ± 8.6	0.335 ± 0.009	0.149 ±0.014	5.7	6.7
M198L	0.401 ± 0.007	–46.9 ± 6.1	0.297 ± 0.007	0.133 ±0.002	5.5	7.3
M198L–T232F	0.382 ± 0.003	–7.51 ± 0.7	0.352 ± 0.007	ND[e]	5.7	6.6
M198L–T232V	0.404 ± 0.004	–29.0 ± 4.2	0.359 ± 0.004	0.145 ±0.030	5.7	6.2

[a]pH 7.0. [b]I_{0V}: Current obtained from CV at 0V. [c]I_{ss}: Steady-state current. [d]DMP activity. [e]ND: not determined.

Replacement of M198 with L caused a modest shift in the acidic direction, the maximum k_{cat} taking place at pH ~7.3. Double variants, M198L–T232V and M198L–T232F exhibited the most dramatic shifts with optimal pH values at ~6.2 and 6.6, respectively. The threonine (T)-to-V replacement yielded higher activity than the T to F replacement. When normalized to the $k_{cat,}$ of the WT the relative activities of T232V, M198L–T232V, T232F, and M198L–T232F were approximately 99, 39, 34, and 7%, respectively. Shifts in optimal pH values and decreased k_{cat} values indicate that the efficiency of the binding step is dictated by the binding pocket environment. Furthermore, replacement of T with F resulted in a decrease in biochemical activity, possibly associated with distortion of the T1 pocket.

The native blue Cu proteins can be transformed into 'green' Cu proteins by replacing the relatively weak axial ligand with a stronger axial ligand or decreasing the distance between the ligand and the reactive T1 Cu atom. Herein, we replaced the weak axial M ligand (M298) with F. A second variant, in which a nearby T residue was replaced by V (M298F–T232V), was also examined. The "blue" native SLAC exhibited an absorbance band at 590 nm and shifts in the LMCT band from the low-energy state to the high-energy state were evidenced by the appearance of an absorbance band at 420 nm for both M298F and M298F–T232V (Figure 5). The double variant exhibited a higher absorbance band ratio than M298F; however, it is not clear that this characteristic is influenced by pH. Both variants retained biochemical and electrochemical activity, although comparison to native SLAC performance revealed a marked decrease.

Replacement of F as in M298F (0.302 V ± 0.005) and M298F–T232V (0.294 V ± 0.018) both exhibited decreased OCP relative to the native SLAC (0.395 V ± 0.007). Given the solid evidence that the coupled distortion model has been demonstrated in the SLAC variants, we propose that replacement of M with F has distorted the T1 binding pocket and forced the Cu atom to interact with the oxygen of a nearby Y residue.

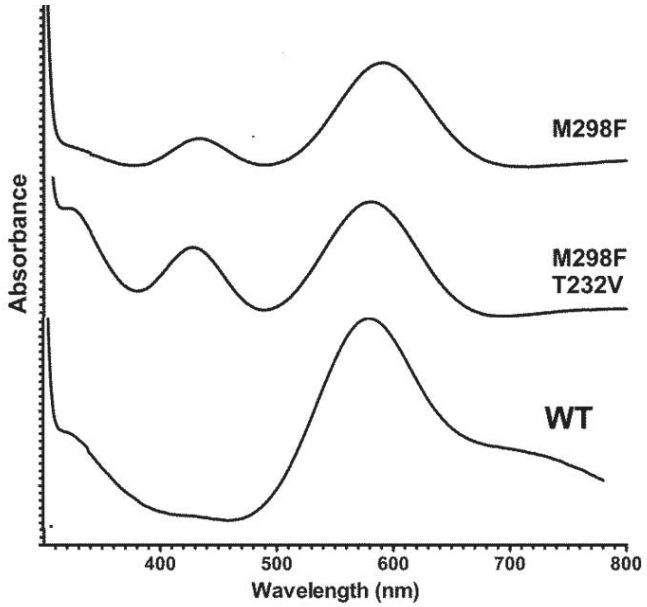

Figure 5: UV–Vis Absorption Spectra of SLAC WT, M298F, and M298F–T232V

Electrochemical studies were performed to assess the electron transfer process characteristics of the SLAC variants. The rate of the electron transfer process, k_{ET}, is dictated by several terms described by the semi-classical Marcus equation [2, 40, 55]. The term H_{AB} is the coupling between the electron donor and acceptor, which can be dictated by the distance between the CNT and the T1 site [53]. In addition, the vibronic, or reorganizational, energy, λ, associated with the protein and the surrounding solvent molecules is considered. Lastly, the driving force, ΔE_0, or the potential difference between the CNT and the T1 site also influences k_{ET}. Moreover, it is important to consider that the overall reaction rate includes not only k_{ET}, but also several other elementary steps, including intramolecular electron transfer between the T1 site and the T2/T3 oxygen reduction site, and a series of steps completing the ORR.

The OCP of the SLAC–BP electrode in oxygen-saturated electrolyte (pH 7.0) was 0.403 V ± 0.001 (Table 2). OCPs of the variants deviated very little from the control (0.382 to 0.404 V). Given that the predicted OCP increase did not occur, the direct bioelectrocatalysis of SLAC was assesed using CV. All of the variants exhibited DET as evidenced by cathodic waves produced in the presence of oxygen. Cathodic current at 0 V was comparable to the WT for T232V, M198L, and M198L–T232V; however, the current density exhibited by variants T232F and M198L–T232F decreased ~sixfold. The decreased bioelectrocatalytic activity associated with the replacement of T232 with F correlates with the observed decreased biochemical activity, indicating that in spite of the differing catalytic mechanisms, the replacement impaired the overall reaction rate. Given the aromaticity of the F moiety, physical interactions (for example, π–π interactions and van der Waals forces) could have distorted the binding pocket enough to decrease k_{ET}.

4.3. Indirectly Establishing the Coupled Distortion Model in SLAC: Transforming a Blue Copper into a Green Copper Protein

Within the SLAC protein, when the ligand increases in strength and/or moves closer to the Cu, a process referred to as coupled distortion can occur [27]. When the axial ligand is weakly coordinated to the Cu, the unique trigonal geometry makes it possible for the $d_{x^2-y^2}$ ground state of Cu(II) to overlap with 4$p\pi$ of the C ligand, resulting in a short Cu–C bond and giving a strong 4$p\pi$(C)-to-Cu LMCT absorbance band at ~600 nm. However, when the axial ligand becomes stronger, the interaction between the ligand and the Cu results in a correspondingly longer Cu–C bond and rotation of the $d_{x^2-y^2}$ ground state of Cu(II) to overlap the 4$p\sigma$ orbital of C. Thus, a more intense 4$p\sigma$(C)-to-Cu^{2+} LMCT absorbance band associated with higher energy (~400 nm) is observed and the 4$p\pi$(C)-to-Cu charge transfer (CT) band at ~600 nm becomes less intense. This coupled distortion results in a strong green color instead of blue. For T1 Cu centers, the relative absorption ratio is a good measure of the strength of axial ligand–Cu interaction.

The stronger axial ligand–Cu interaction has been shown to lower the redox potential of the T1 Cu center [34]. In 2010, Clark, *et al*., replaced the weak M axial ligand with a relatively stronger C ligand, which resulted in an optical transition favoring the higher energy LMCT and a decrease in redox potential of ~0.1 V [34]. Conversely, Basumalick, *et al*.—using a green Cu nitrite reductase—replaced a relatively strong M axial ligand with T and converted the green Cu site into a blue Cu site [33]. In this case, the M axial ligand induced the coupled distortion, underlining the importance of not only the presence and identity of the ligand, but also the distance between the ligand and the Cu center and indirect effects caused by protein conformation [30, 32].

In previous work, replacement of a relatively strong axial ligand with a weaker one resulted in a lessening of the coupled distortion effect. In this case, replacement of the axial ligand with a hydrophobic residue *induced* the coupled distortion effect. A plausible explanation is that the physical bulkiness of F has pushed the Cu, causing it to form a new axial ligand with a nearby polar residue (or moiety). A good axial ligand candidate is the hydroxyl group found on T230, which is situated opposite to the axial M298 and is close enough to interact with Cu (Figure 1). In addition, the F could interact—via π–π interactions or van der Waals—with the binding pocket and induce a rearrangement that favors the lengthening of the Cu–C ligand. The double variant, M298F–T232V, exhibits optical evidence (a higher R_L) that it favors the $p\sigma$(C)-to-Cu^{2+} LMCT band, which indicates that the binding pocket could be rearranging more than the single variant's (M298F) binding pocket.

4.3.1. UV-Vis Spectral Characterization of Green SLAC Variants

The UV–Vis spectra of SLAC variants M298F and M298F–T232V, along with that of WT SLAC, were compared to confirm that the blue and green appearance of each protein preparation corresponded to an absorbance band at ~600 nm associated with the T1 coordination sphere of the WT and an additional absorbance band at ~400 nm associated with distortion of the T1 coordination sphere in the two variants. At pH 7.0, the WT spectrum revealed a maximum absorbance at 590 nm, which correlates with the low-energy region, the 4$p\pi$(C)-to-Cu CT band (Figure 5) in good agreement with those obtained for similar proteins [26, 27, 30, 34]. Spectra of

the M298F and M298F–T232V variants exhibited a second absorbance peak at 420 nm, associated with a higher 4*pσ*(C)-to-Cu CT band, which suggests that an axial ligand stronger than the removed M ligand is inducing the trend predicted by the coupled distortion model. It should be noted that the double variant, M298F–T232F, did not exhibit absorbance in the visible spectrum and did not exhibit catalytic activity (biochemical or electrochemical). Given that both CT bands are observed when the axial ligand is removed and replaced by an F residue, the ratio of the two absorbance peaks (i.e., the ratio of the high-energy state to the low-energy state), R_L, can be an indicator of the extent of the contribution from each CT state; a low R_L indicates more contribution from the 4*pπ*(C)-to-Cu CT state, and a high R_L is indicative of more contribution from the 4*pσ*(C)-to-Cu CT state and lengthening and weakening of the Cu–C bond. Furthermore, deprotonation of the chemical moiety serving as the axial ligand could enhance the Cu–C bond and increase R_L [34]. A pH titration of M298F and of M298F–T232V revealed an increase in R_L for M298F as pH increased from 6 to 9 (Figure 6).

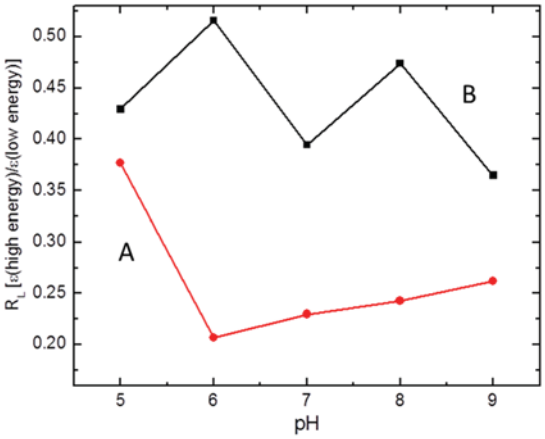

Figure 6: R_L Values Obtained for M298F (A) and M298F-T232V (B) at pH 5–9

The stronger interaction with Cu(II) in basic conditions points toward an amino acid residue or chemical moiety with pK_a > 9; for example, Y has pK_a ~10. Compared to M298F, M298F–T232V exhibited a higher R_L at all pH values and did not demonstrate a discernible trend, suggesting that several factors contribute to the interaction between the ligand and the Cu(II) center. According to Machczynski, et al., the predicted pI (isoelectric point) of the apoenzyme is 6.2, whereas pI of the Cu(II) form is 8.2 [23]. It is also possible that the double variant is less stable than the single variant.

4.3.2. Biochemical and Electrochemical Activity of Green SLAC Variants

In 2004, Machczynski, et al. reported that SLAC exhibited optimal catalytic turnover rate, k_{cat}, at pH ~8.0 [23]. Given that the ORR requires acidic conditions to flourish, this atypical catalytic performance is explained by a decreased K_M in basic conditions. Hence, catalytic efficiency, k_{cat}/K_M, is highest at pH ~9.0. This is likely due to abundant hydrophobic residues in the T1 binding cleft and the pK_a of DMP and binding pocket Y residues. Our experimentally determined WT k_{cat} is in good agreement with the previous Machczynski report, with a maximum that occurs at pH ~7.7 [23]. Optimal activity for M298F and M298F–T232V exhibited a modest shift in the basic direction and was determined to take place at pH ~7.8 and 8.1, respectively (Table 3).

However, k_{cat} decreased for both M298F and M298F–T232V and was roughly 9% and 1%, respectively, of WT SLAC. Retention of the basic k_{cat} pH indicates that the efficiency of the binding step dictated the reaction rate in spite of the overall catalytic impairment caused by distortion of the catalytic site.

Table 3: pH Optima of WT SLAC and "Green" SLAC Variants
Based on DMP Activity and Electrochemical Activity (OCP at pH 7.0)

	WT	M298F	M298F–T232V
k_{cat} pH optimum[a]	7.7	7.8	8.2
I_{ss} pH optimum[b]	5.6	5.0	5.1
OCP (V)[c]	0.395 ± 0.007	0.302 ± 0.005	0.294 ± 0.018

[a]DMP activity. [b]I_{ss}: Steady-state current. [c]pH 7.

The OCP of the SLAC–BP electrode in oxygen-saturated electrolyte (pH 7.0) was 0.395 ± 0.007 V (Table 3). OCPs for the M298F and M298F–T232V variants decreased to 0.302 ± 0. 005 V and 0.294 ± 0.018 V, repectively (Table 3) (Appendix A). This ~0.1 V decrease is in good agreement with previous work and can be related to the energy level of the $d_{x^2-y^2}$ orbital [34]; when the energy of the highest $d\pi$ level is lower, the energy of the ligand field increases and results in a higher reduction potential [28]. Direct bioelectrocatalysis was demonstrated by obtaining CV in the presence of oxygen for the WT and the M298F and M298F–T232V variants (Figure 7). Both variants exhibited modest cathodic current indicative of ORR and DET to the T1 site.

Steady-state current densities were obtained in the pH range 4.2–9.0 for the WT and the M298F, and M298F–T232V variants and optimal bioelectrocatalytic activity was found to occur at pH 5.6, 5.0, and 5.1, respectively. This optimal activity agrees well with a previously published report that characterized the electrochemical activity of SLAC in the presence of an osmium-complex mediator [24]. Reduction of the T1 Cu site takes place via electron tunneling and this process differs from the DMP oxidation mechanism: in direct bioelectrocatalysis, the three terms outlined by Marcus theory—H_{AB}, λ, ΔE^0— play a prominent role and formation of the enzyme–substrate follows the Michaelis–Menten model. Optimal bioelectrocatalytic activity decreased to ~8% and ~10% of the WT activty for M298F and M298F–T232V, respectively; this activity decrease is in good agreement with activity trends revealed by DMP assays.

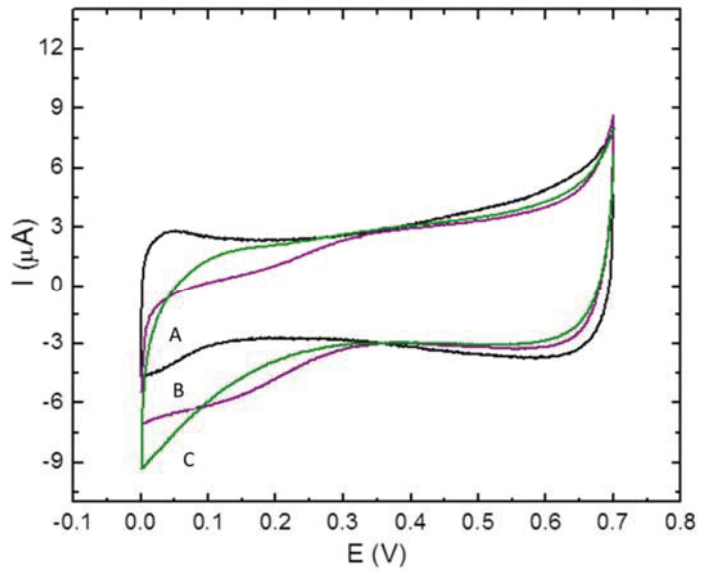

Figure 7: CV of BP (A), with M298F (B), and with M298F–T232V (C)
Measurements in Oxygen-Saturated Electrolyte; pH = 5.0; Scan Rate = 5 mV sec^{-1}

4.4. SLAC Variants Tailored to Interface with AuNPs

DET between the T1 Cu center and a conductive surface occurs when the distance between the catalytic center and the electrode is reduced enough to enable effective electron tunneling. Although there are numerous reports in which carbon electrodes have performed direct bioelectrocatalysis, DET between MCOs and gold surfaces has been demonstrated to a lesser extent [34, 35]. Efficient immobilization along with the orientation of the redox center on the surface of gold could serve to enhance the DET process. One way to accomplish both immobilization and favorable orientation of SLAC simultaneously is to replace a solvent-accessible residue near the T1 binding pocket with a C residue. The sulfur moiety of C will bind to the gold surface, essentially anchoring SLAC on the surface of the gold. Herein, a variant of SLAC was evaluated for interaction with a gold surface via specific addition of a C residue (Y229C). Replacement of the solvent-accessible Y residue near the T1 binding pocket resulted in specific interaction between SLAC and AuNPs via the available thiol. Verification of the specific interaction was achieved by suspending Y229C with AuNPs and subjecting the suspension to gel electrophoresis and UV-vis absorbance measurements. The migration of colloidal gold along an agarose gel in the presence of an applied voltage requires the modification of the AuNPs with a capping agent or charged group. Proteins are large, charged, amphiphilic molecules able to coat AuNPs via nonspecific interactions. Therefore, mixing protein suspensions with AuNPs will result in coated particles capable of migration on an agarose gel. Given that the protein will nonspecifically interact with the particle, a blocking molecule, DTT, is introduced into the suspension [47]. DTT interacts with gold via the thiol moiety and blocks proteins from the gold surface. DTT also reduces disulfide bonds to thiols; exposure to DTT prevents Y229C from forming disulfide bonds with other SLAC assemblies (monomers, dimers, or trimers). Figure 8 shows the migration of SLAC–AuNP suspensions on an agarose gel. When WT SLAC was incubated with DTT, the AuNPs did not migrate along the gel; however, in the absence of DTT,

the particles migrate and exhibit a characteristic red band associated with AuNPs. A suspension of AuNP and Y229C, however, migrates along the gel, regardless of the presence or absence of DTT. This observation can be explained by a decrease in *non*specific interactions between Y229C and the AuNPs.

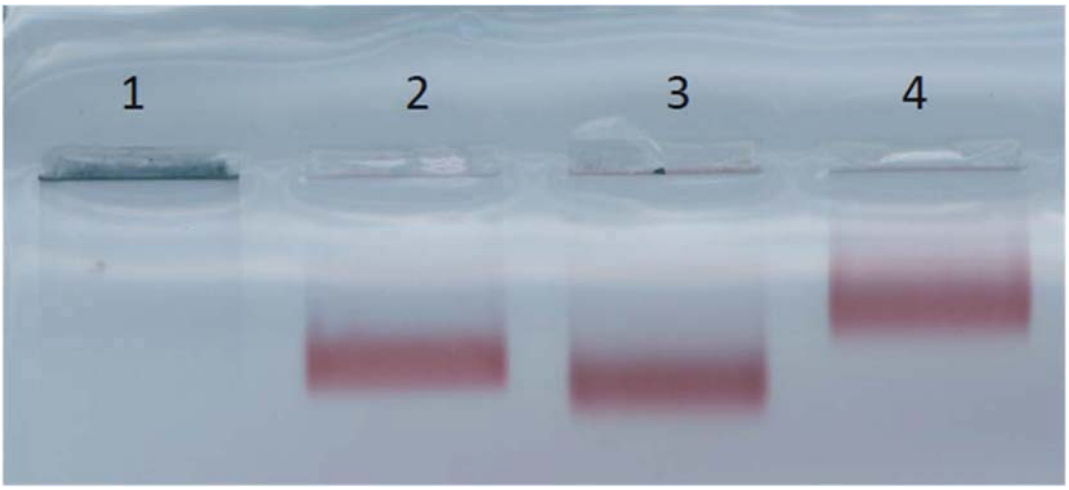

Figure 8: Gel Electrophoresis of SLAC–AuNP Suspensions
Key: Lanes 1 and 2 are WT SLAC pre-incubated with and without DTT, respectively. Lanes 3 and 4 are Y229C pre-incubated with and without DTT, respectively

5. CONCLUSIONS

The catalytic center of SLAC comprises three Cu sites: The T1 Cu site accepts electrons from an electron donor and transfers them to the T2/T3 cluster, where O_2 is reduced to H_2O in a four-electron reaction. Molecular and dynamic simulations comparing SLAC to other MCOs with higher T1 redox potentials (ε^0) predicted mutations that would exhibit an increased T1 Cu redox potential. Quantum mechanics/molecular mechanics and molecular dynamics simulations predicted ε^0 for four MCOs, including SLAC, and were used to identify mutations likely to increase the T1 potential. M198L (M198 replaced with L) and T232V (T232 replaced with V) were selected and characterized based on DMP activity and bioelectrocatalytic performance.

Recombinant expression of SLAC was achieved in *E. coli* in an effort to generate a uniform preparation of purified SLAC protein. Similar to the prior studies, a pET system vector was used for expression, but with additional deletions at the 5′ and 3′ ends of the gene that eliminate post-translational modifications that occur after production of the enzyme. Codon usage of the gene was optimized for enhanced expression in *E. coli* and a His-tag affinity system was adopted for ease of purification. The purification procedure resulted in consistent and reproducible active preparations of SLAC with purity typically >70%.

SLAC activity assays using DMP as the electron donor revealed optimal-pH shifts toward acidic values. WT SLAC exhibited an optimal activity at pH ~7.7, and M198L, T232V, and M198L–T232V (double mutant) revealed optimal activity at pH ~7.4, ~6.6, and ~6.6, respectively. The OCP with respect to Ag/AgCl reference electrodes did not reveal a significant change in ε^0 when SLAC was immobilized on CNT electrodes; however current density for M198L was higher than for the WT, especially when the purity of the protein preparation was taken into account. Half-wave potentials ($E_{1/2}$)—for M198L, T232V, and M198L-T232V—were comparable or slightly higher than for the WT; this was confirmed in both quiescent conditions and on rotating disc electrodes (RDEs) (Appendix B). RDE experiments using platinum rings detected H_2O_2 production, indicating either a two-electron reduction process or multiple electron transfer mechanisms. Future studies are needed to verify the three-dimensional stability of SLAC and the interaction between the T1 Cu site and the surface of the electrode. Furthermore, the continuation of this study can enhance fundamental knowledge regarding structure–function relationships of MCOs and superior strategies for technological development. Work in this area continues and recent reports document findings that agree with our observations and apply alternative approaches, such as paramagnetic NMR, to elucidate the mechanisms of electron transfer within SLAC [36–39].

Direct bioelectrocatalysis of the purified SLAC protein was evaluated on BP electrodes with WT SLAC and seven SLAC variants. Further studies could shed light on DET and provide insight into approaches to maximize current density and enhance the electrode fabrication process. Enzymatic bioelectrodes offer advantages in catalytic specificity and could potentially enable useful Air Force applications. However, power density of an EFC is still 2~3 orders of magnitude lower than that of chemical fuel cells, amongst other known limitations. Although promising approaches for stable and efficient bioelectrodes have been proposed, there are still barriers to effective enzyme-modified

electrodes that need to be addressed. The variant proteins described herein may expand/improve the suite of ORR biocatalysts for EFC. If that advance is achieved, it may provide a technological breakthrough that could be used in large-scale applications for “stand-alone” energy supplies.

6. REFERENCES

1. Luckarift HR, Atanasov P, and Johnson GR. In: Luckarift HR, Atanasov P, and Johnson GR eds. *Enzymatic Fuel Cells: From Fundamentals to Applications*. John Wiley & Sons; 2014:1–3.
2. Marcus RA, and Sutin N. Electron transfers in chemistry and biology. *Biochim. Biophys. Acta.* 1985;811(3):265–322.
3. Ramasamy RP, Luckarift HR, Ivnitski DM, Atanassov PB, and Johnson GR. High electrocatalytic activity of tethered multicopper oxidase-carbon nanotube conjugates. *Chem. Comm.* 2010;46 (33):6045–6047.
4. Strack G, Luckarift HR, Nichols R, Cozart K, Katz E, and Johnson GR. Bioelectrocatalytic generation of directly readable code: harnessing cathodic current for long-term information relay. *Chem. Comm.* 2011;47 (27):7662–7664.
5. Hussein L, Urban G, and Kruger M. Fabrication and characterization of buckypaper-based nanostructured electrodes as a novel material for biofuel cell applications. *Phys. Chem. Chem. Phys.* 2011;13 (13):5831–5839.
6. Hussein L, Rubenwolf S, von Stetten F, Urban G, Zengerle R, Krueger M, and Kerzenmacher S. A highly efficient buckypaper-based electrode material for mediatorless laccase-catalyzed dioxygen reduction. *Biosens. Bioelectron.* 2011;26 (10):4133–4138.
7. Narvaez Villarrubia CW, Rincon RA, Radhakrishnan VK, Davis V, and Atanassov P. Methylene green electrodeposited on SWNTs-based "bucky" papers for NADH and l-malate oxidation. *ACS Appl. Mater. Inter.* 2011;3 (7):2402–2409.
8. Strack G, Luckarift HR, Sizemore SR, Nichols RK, Farrington KE, Wu PK, Atanassov P, Biffinger JC, and Johnson GR. Power generation from a hybrid biological fuel cell in seawater. *Bioresource Technol.* 2013;128: 222–228.
9. Rincon RA, Lau C, Luckarift HR, Garcia KE, Adkins E, Johnson GR, and Atanassov P. Enzymatic fuel cells: integrating flow-through anode and air-breathing cathode into a membrane-less biofuel cell design. *Biosens. Bioelectron.* 2011;27 (1):132–136.
10. Strack G, Nichols R, Atanassov P, Luckarift HR, and Johnson GR. Modification of carbon nanotube electrodes with 1-pyrenebutanoic acid, succinimidyl ester for enhanced bioelectrocatalysis *Methods in Molecular Biology: Immobilization of enzymes and cells; Humana Press.* 2013;217–228.
11. Skálová T, Dohnálek J, Østergaard LH, Østergaard PR, Kolenko P, Dušková J, Štěpánková A, and Hašek J. The structure of the small laccase from *Streptomyces coelicolor* reveals a link between laccases and nitrite reductases. *J. Mol. Biol.* 2009;385:1165–1178.
12. Dubé E, Shareck F, Hurtubise Y, Daneault C, and M B. Homologous cloning, expression, and characterisation of a laccase from *Streptomyces coelicolor* and enzymatic decolourisation of an indigo dye. *App. Micro. Biotechnol.* 2008;79 (4):597–603.
13. Barton SC, Gallaway J, and Atanasov P. Enzymatic biofuel cells for implantable and microscale devices. *Chem. Rev.* 2004;(104):4867–86.
14. Heller A. Miniature biofuel cells. *Phys. Chem. Chem. Phys.* 2004;(6):209–216.
15. Heller A. Potentially implantable miniature batteries. *Anal. Bioanal. Chem.* 2006; 385:469–73.
16. Mano N, Mao F, and Heller A. A miniature biofuel cell operating in a physiological buffer. *J. Am. Chem. Soc.* 2002;124 (44):12962–12963.

17. Meredith MT, and Minteer SD. Biofuel cells: enhanced enzymatic bioelectrocatalysis. *Ann. Rev. Anal. Chem.* 2012;5:157–179.
18. Quintanar L, Stoj C, Taylor AB, hart PJ, Kosman DJ, and Solomon EI. Shall we dance? How a multicopper oxidase chooses its electron transfer partner. *Acc. Chem. Res.* 2007;40 (6):445–452.
19. Hong G, Ivnitski DM, Johnson GR, Atanassov P, and Pachter R. Design parameters for tuning the type 1 Cu multicopper oxidase redox potential: insight from a combination of first principles and empirical molecular dynamics simulations. *J. Am. Chem. Soc.* 2011;133(13):4802–4809.
20. Vaz-Dominguez C, Campuzano S, Rudiger O, Pita M, Gorbacheva M, Shleev S, Fernandez VM, and De Lacey AL. Laccase electrode for direct electrocatalytic reduction of O2 to H2O with high-operational stability and resistance to chloride inhibition. *Biosens. Bioelectron.* 2008;24 (4):531–537.
21. Shleev S, Christenson A, Serezhenkov V, Burbaev D, Yaropolov A, Gorton L, and Ruzgas T. Electrochemical redox transformations of T1 and T2 copper sites in native *Trametes hirsuta* laccase at gold electrode. *Biochem. J.* 2005;385:745–754.
22. L. Betancor, Johnson GR, and Luckarift HR. Stabilized heterogeneous laccases in bioelectrocatalysis. *ChemCatChem.* 2013;5 (1):46–60.
23. Machczynski M, Vijgenboom E, Samyn B, and Canters G. Characterization of SLAC: a small laccase from *Streptomyces coelicolor* with unprecedented activity. *Protein Sci.* 2004;13:2388–2397.
24. Gallaway J, Wheeldon I, Rincon R, Atanasov P, Banta S, and Barton SC. Oxygen-reducing enzyme cathodes produced from SLAC,a small laccase from *Streptomyces coelicolor*. *Biosens. Bioelectron.* 2008;23;1229–1235.
25. Trohalaki S, Pachter R, Luckarift HR, and Johnson GR. Immobilization of the Laccases from *Trametes versicolor* and *Streptomyces coelicolor* on Single-wall Carbon Nanotube Electrodes: A Molecular Dynamics Study. *Fuel Cells.* 2012;12 (4):656–664.
26. LaCroix LB, Shadle SE, Wang Y, Averill BA, Hedman B, Hodgson KO, and Solomon EI. Electronic structure of the perturbed blue copper site in nitrite reductase: spectroscopic properties, bonding, and implications for the entatic/rack state. *J. Am. Chem. Soc.* 1996;118(33):7788–7769.
27. Solomon EI. Spectroscopic methods in bioinorganic chemistry: blue to green to red copper sites. *Inorg. Chem.* 2006;45:8012–8025.
28. Malmstrom B. Rack-induced bonding in blue-copper proteins. *Eur. J. Biochem.* 1994;223:711–718.
29. Pierloot K, De Kerpel JOA, Ryde U, Olsson MHM, and Roos BO. Relation between the structure and spectroscopic properties of blue copper proteins. *J. Am. Chem. Soc.* 1998;120:13156–13166.
30. Randall DW, Gamelin DR, LaCroix LB, and Solomon EI. Electronic structure contributions to electron transfer in blue Cu and CuA. *J. Bio. Inorg. Chem.* 2000;5:16–19.
31. Lu Y, LaCroix LB, Lowery MD, Solomon EI, Bender CJ, Peisach J, Roe JA, Gralla EB, and Selverstone Valentine J. Construction of a blue copper site at the native zinc site of yeast copper-zinc superoxide dismutase. *J. Am. Chem. Soc.* 1993;115(14):5907–5918.

32. Pascher T, Karlsson BG, Nordling M, Malmstrom BG, and Vanngard T. Reduction potentials and their pH dependence in site-directed-mutant forms of azurin from *Pseudomonas aeruginosa*. *Eur. J. Biochem.* 1993;212:289–296.
33. Basumallick L, Szilagyi RK, Zhao Y, Shapleigh JP, Scholes CP, and Solomon EI. Spectroscopic studies of the Met182Thr mutant of nitrite reductase: role of the axial ligand in the geometric and electronic structure of blue and green copper sites. *J. Am. Chem. Soc.* 2003;125(48):14784–14792.
34. Clark KM, Yu Y, Marshall NM, Sieracki NA, Nilges MJ, Blackburn NJ, van der Donk W, and Lu Y. Transforming a blue copper into a red copper protein: engineering cysteine and homocysteine into the axial position of azurin using site-directed mutagenesis and expressed protein ligation. *J. Am. Chem. Soc.* 2010;132(29):10093–10101.
35. Reed AMW, and Metallo SJ. Oriented protein adsorption to gold nanoparticles through a genetically encodable binding motif. *Langmuir.* 2010;26(24):18945–18950.
36. Surwase SV, Patil SA, Srinivas S, and Jadhav JP. Interaction of small molecules with fungal laccase: A Surface Plasmon Resonance based study. *Enz. Microb. Technol.* 2016;82:110–4.
37. Machczynski MC, and Babicz JT, Jr. Correlating the structures and activities of the resting oxidized and native intermediate states of a small laccase by paramagnetic NMR. *J. Inorg. Biochem.* 2016;159:62–69.
38. Prins A, Kleinsmidt L, Khan N, Kirby B, Kudanga T, Vollmer J, Pleiss J, Burton S, and Le Roes-Hill M. The effect of mutations near the T1 copper site on the biochemical characteristics of the small laccase from *Streptomyces coelicolor* A3(2). *Enz. Microb. Technol.* 2015;68:23–32.
39. Guan D, Kurra Y, Liu W, and Chen Z. A click chemistry approach to site-specific immobilization of a small laccase enables efficient direct electron transfer in a biocathode. *Chem. Comm.* 2015;51(13):2522–2525.

Appendix A: ELECTROCHEMICAL CHARACTERIZATION OF WT AND VARIANTS OF SLAC

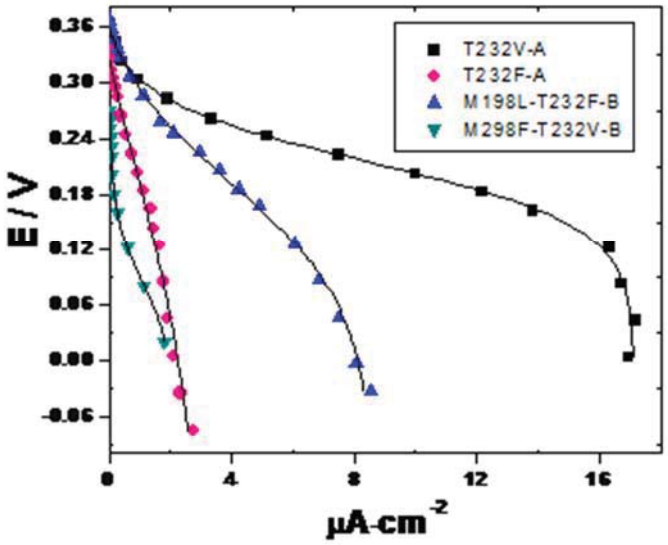

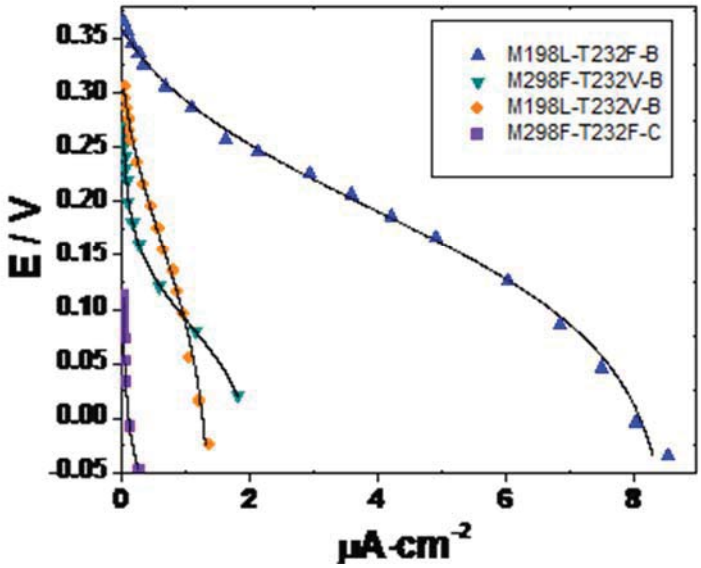

WT	T232V	T232F	M198L-T232F	M198L-T232V	M298F-T232V	M298F-T232F
395 ± 7	381 ± 6	363 ± 2	389 ± 3	341 ± 11	294 ± 18	199 ± 13

OCP (mV)

Figure A1: Polarization Curves of WT and Variants of SLAC

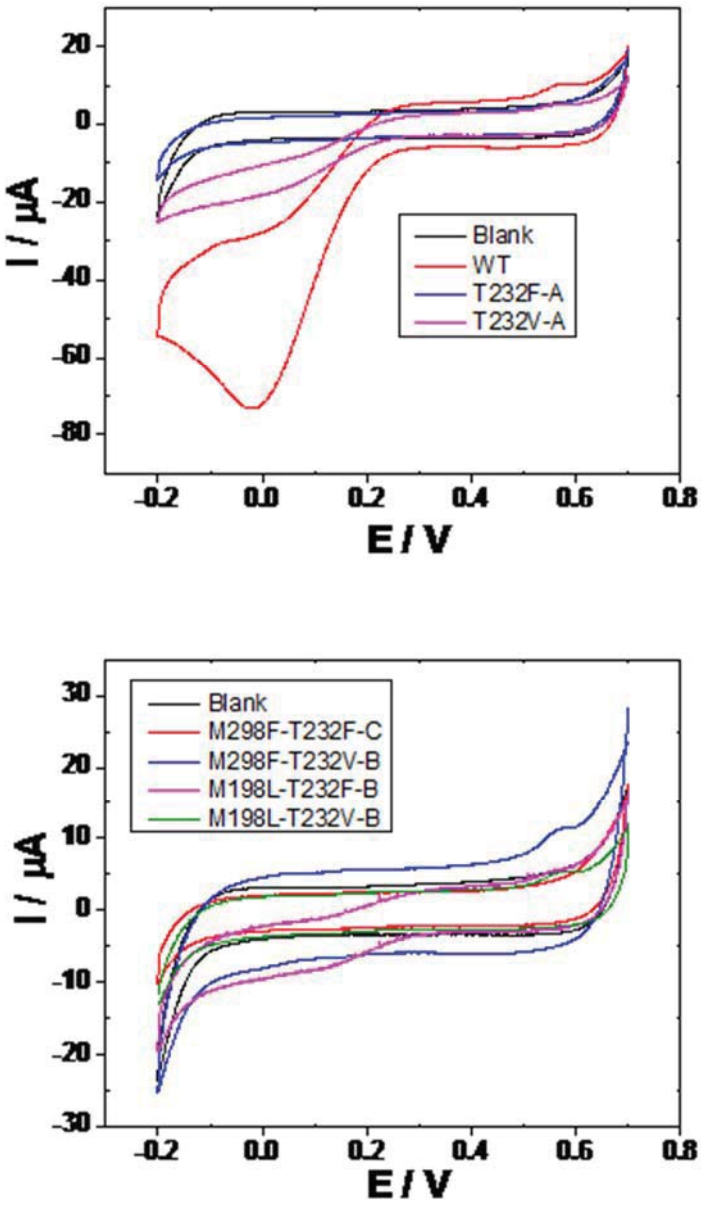

Figure A2: CV for WT and Variants of SLAC

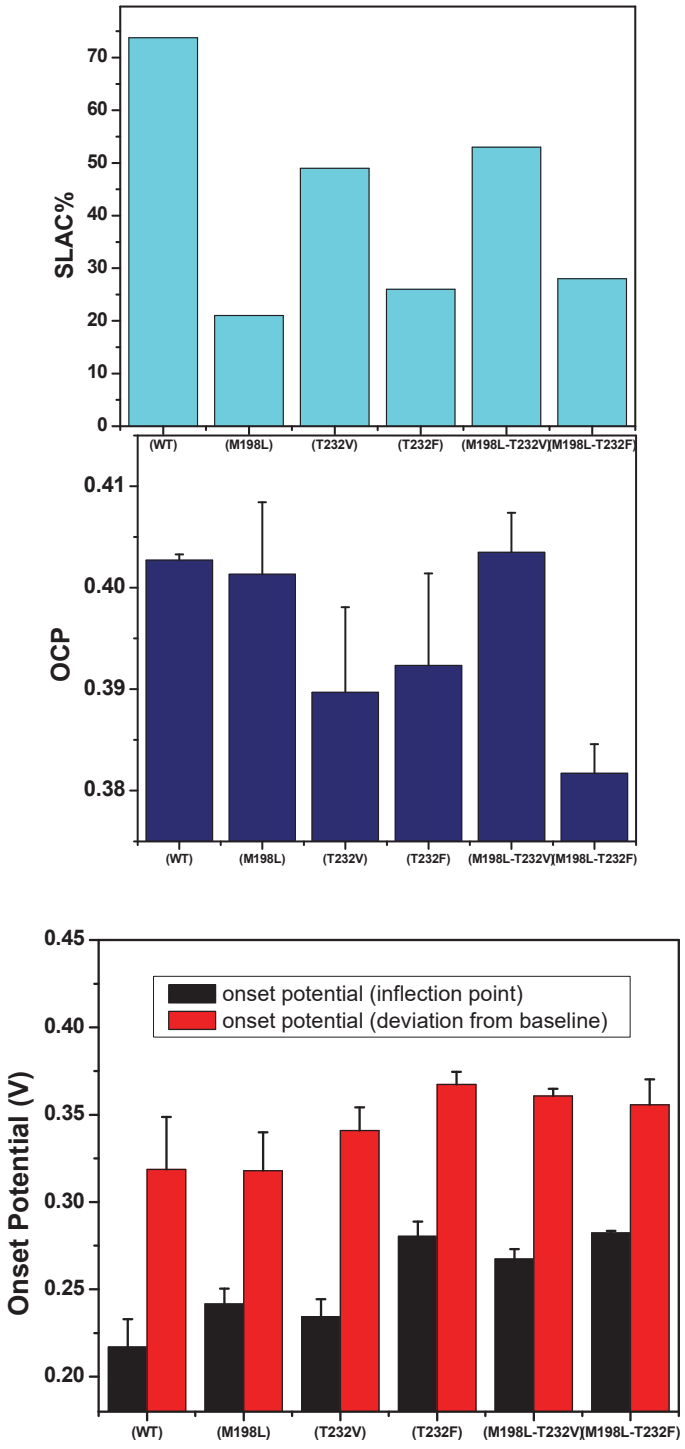

Figure A3: Characteristics of WT and Variants of SLAC
Top: Purity of protein preparation (%); center: OCP (mV); bottom: onset potential (V)

Appendix B: ROTATING DISK ELECTRODE (RDE) STUDIES OF WT AND VARIANTS OF SLAC

Electrochemical data provided by Sofia Babanova, UNM
RDE is a hydrodynamic working electrode used in a conventional three-electrode system. Herein, the RDE approach was used for WT SLAC and all variant SLACs; measurements are reported vs. 3M Ag/AgCl reference electrode with a Pt wire as the counter electrode.

The half-wave potential of WT SLAC was determined to be 155 mV, by taking the first derivative of the polarization curve at rotation speeds of 1600 rpm (Figure B1). There is an observable difference in generated current when using an RDE compared to a stationary electrode. Due to slow kinetics, however, saturation is not reached.

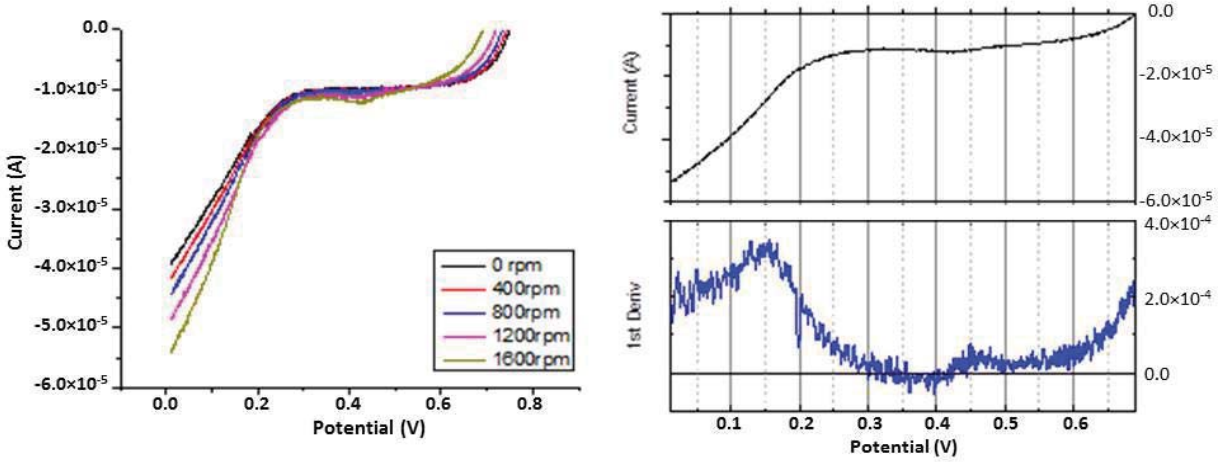

Figure B1: RDE Measurements of WT SLAC

There is an extremely small difference between the currents observed at the different rotating speeds, due to the fact that the enzyme does not attain the diffusional limit because of the poor kinetics. The half-wave potential for T232F is 170 mV, which is higher than the $E_{1/2}$ of the WT (Figure B2). However, its observed current is ~ 4x lower than for the WT.

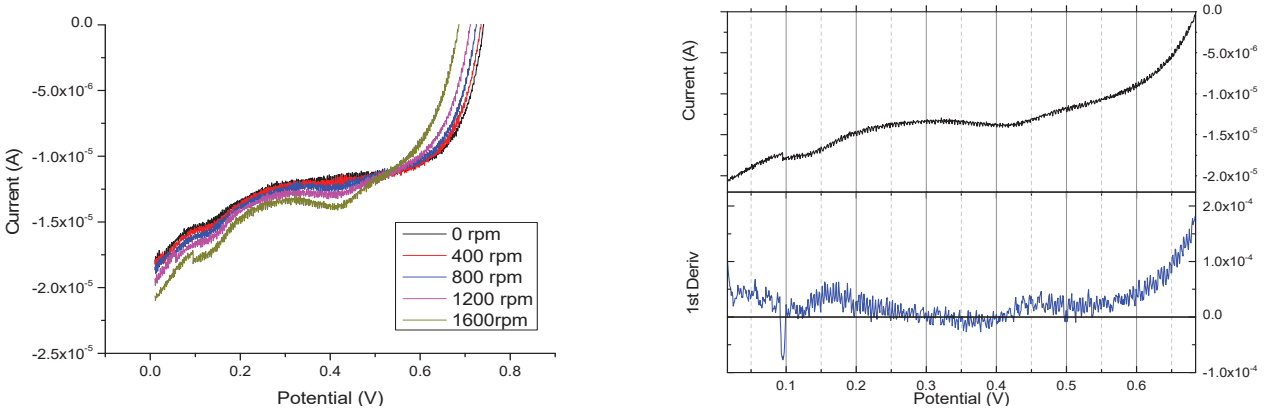

Figure B2: RDE Measurements of T232F SLAC Variant

The same conclusion can be drawn for mutant T232V as for T232F (Figure B3). The currents that these two mutants produce, when normalized to enzyme loading, are statistically identical (-56.5 µA/mg for T232F and -52.9 µA/mg for T232V). This indicates that the replacement of T with V and/or F is shifting $E_{1/2}$ to more positive values, but lowers the overall activity of the enzyme. When the hydroxyl group of the amino acid at the 232 position is removed, the overall activity drops, but the type of amino acid (V or F) does not appear to play a significant role. This raises the question does the hydroxyl group lie close to the T1 center or coordinate directly with Cu from the T2/T3 center.

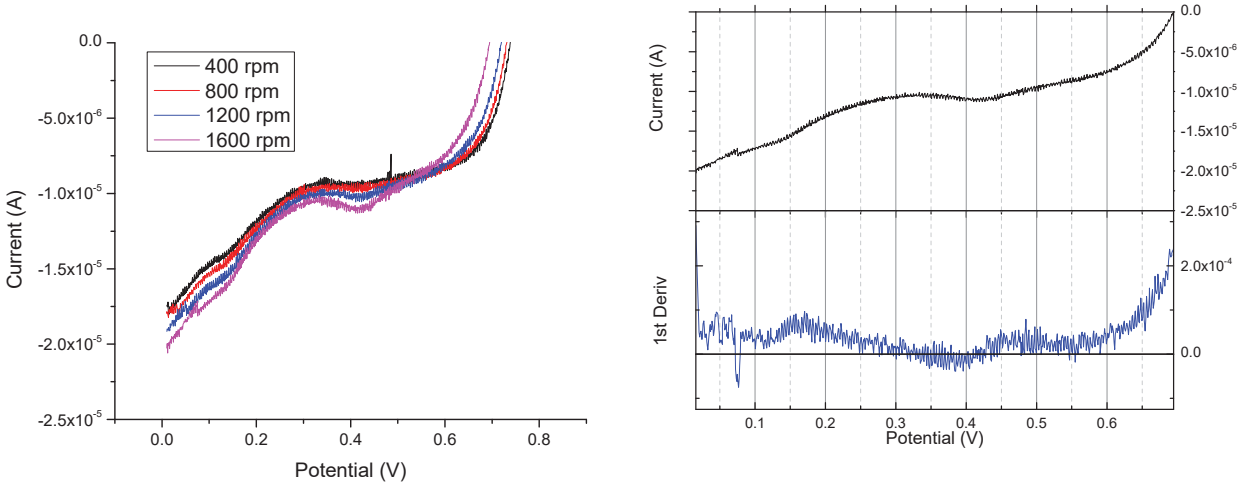

Figure B3: RDE Measurements of T232V SLAC Variant

Mutation M198L does not statistically change the half-wave potential, 155 mV (± 5 mV), relative to the WT; however, it had the highest activity of all the variants characterized (Figure B4).

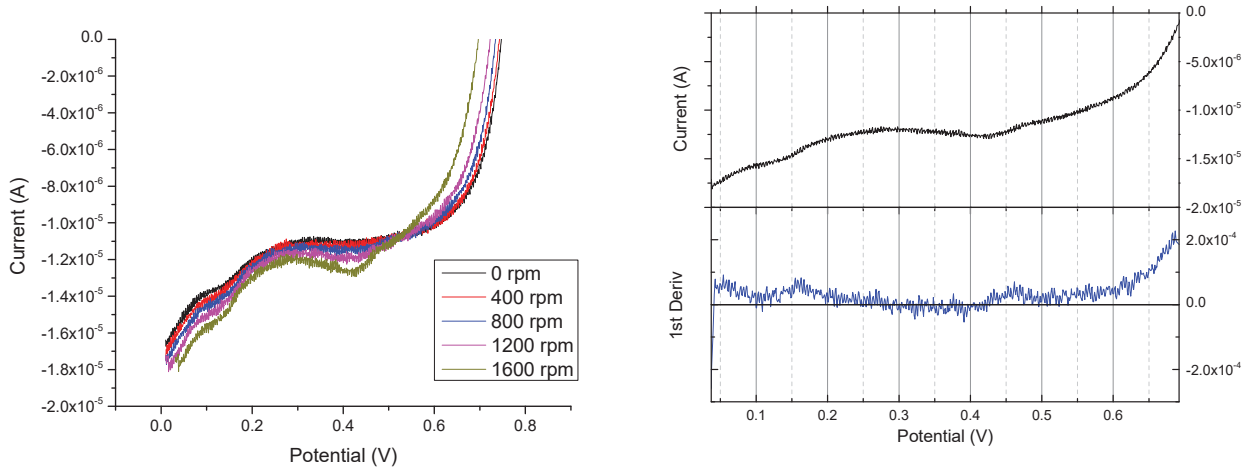

Figure B4: RDE Measurements of M198L SLAC Variant

The $E_{1/2}$ of M298F-T232V is equivalent to the single mutants' in which T was replaced (170 mV) (Figure B5). The activity of this double mutant is slightly higher than that observed for the single variant T232V.

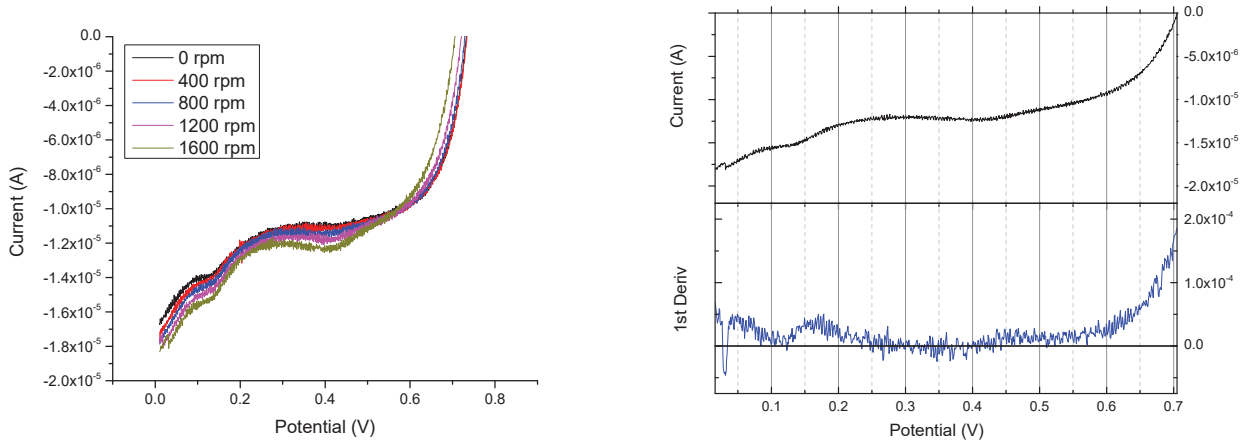

Figure B5: RDE Measurements of M298F-T232V SLAC Variant

For the double variant M198L-T232F, we theorize that the M198L mutation is dominant and as a result produces results comparable to those of the single mutant M198L (Figure B6).

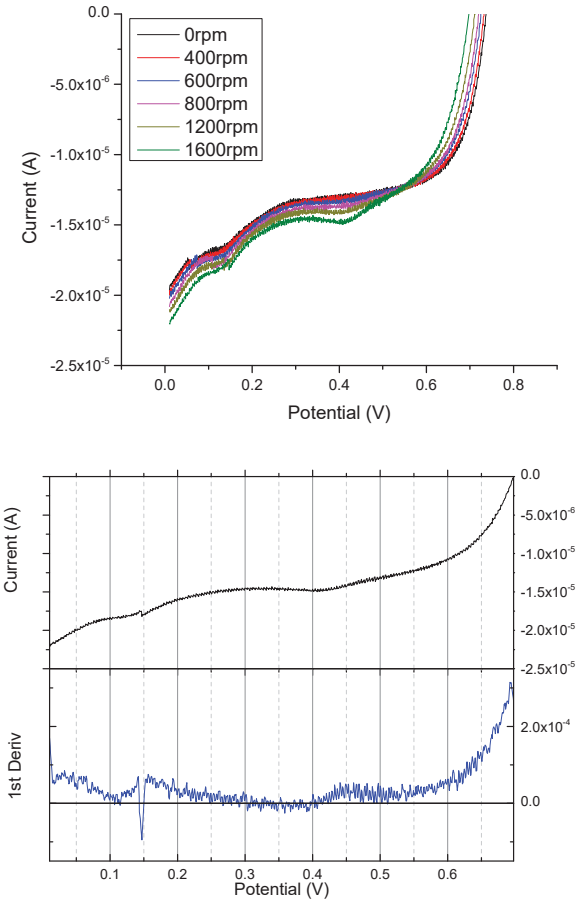

Figure B6: RDE Measurements of M198L-T232F SLAC variant

In the case of the double variant M198L-T232V the influence of both mutations can be seen: higher $E_{1/2}$ and comparatively lower enzyme activity in comparison with the single T232V mutant (Figure B7).

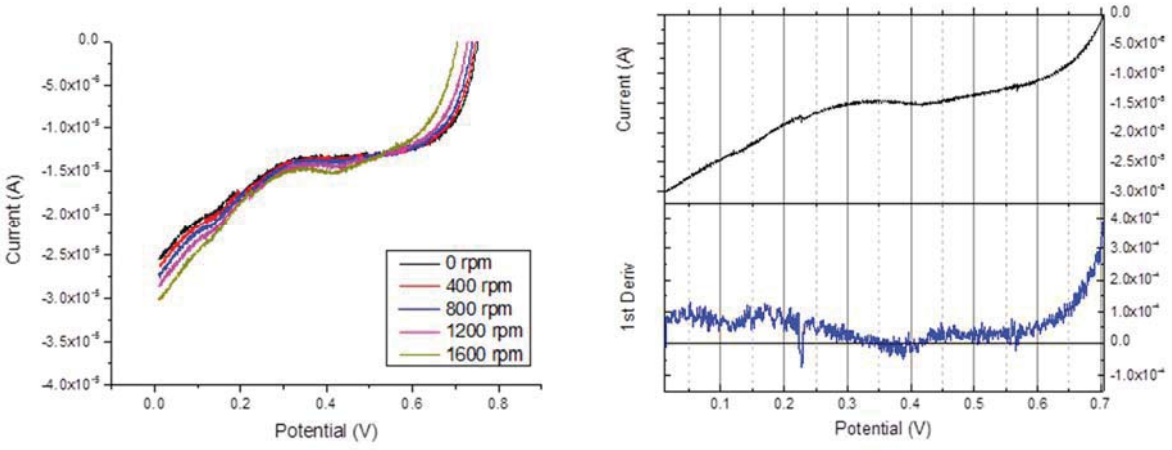

Figure B7: RDE Measurements of M198L-T232V SLAC Variant

Comparison of WT and SLAC variants

Figure B8 represents the WT and SLAC results directly as recorded. Even though the procedure is optimized, the surface area of the electrode after CNT deposition can vary, and some of the observed differences may be attributed to differences in surface area. In addition, protein loadings are not equal for each variant.

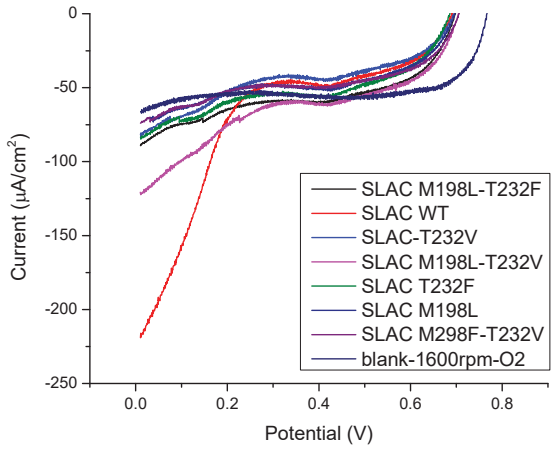

Figure B8: RDE of WT and SLAC variants

Figure B9 shows the data with capacitance subtracted. It can now be seen that the double mutant M198L-T232V has a higher onset potential and higher current, amongst all the mutants tested. It must be noted, however, that the loading of this mutant is approximately two times higher.

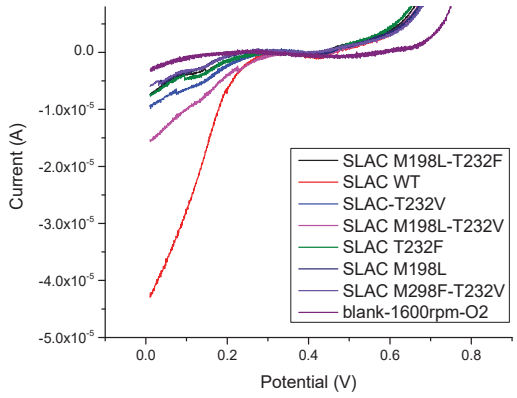

Figure B9: RDE (with capacitance subtracted) of WT and SLAC variants

Finally, Figure B10 represents the data with the capacitance subtracted and the current normalized to enzyme loading. All data is summarized in Table 1.

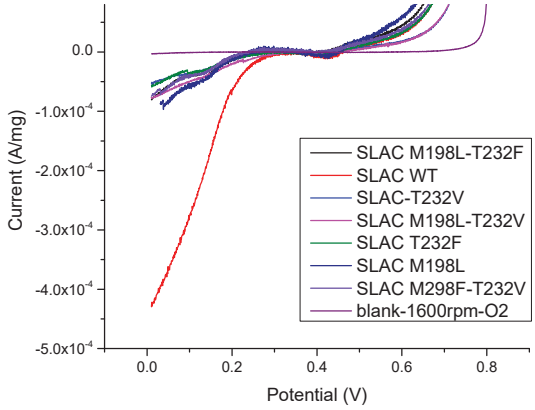

Figure B10: RDE Measurements (with Capacitance Subtracted) of WT and SLAC Variants, Normalized to Enzyme Loading

Table B1. Summary of RDE electrode potentials

	Enzyme loading (mg)	$\Delta I_{0.35V\text{-}0V}$(μA mg^{-1})	$E_{1/2}$(mV)
MWCNT (control)	0	0	N/A
WT	0.10	-429.4	155
T232F	0.13	-56.5	170
T232V	0.18	-52.9	170
M198L	0.06	-86.8	160
M298F-T232V	0.08	-74.3	170
M198L-T232F	0.09	-82.6	156
M198L-T232V	0.20	-76.4	170

LIST OF SYMBOLS, ABBREVIATIONS, AND ACRONYMS

°C	degrees Celsius
Ag/AgCl	silver/silver chloride
AuNP	gold nanoparticle
BP	buckypaper
C	cysteine (Cys)
CNT	carbon nanotube
CT	charge transfer
Cu	Copper
CV	cyclic voltammetry
DET	direct electron transfer
DMP	2,6-dimethoxyphenol
DMSO	dimethylsulfoxide
DTT	dithiothreitol
$E_{1/2}$	Half-cell potential
EDTA	ethylenediaminetetraacetic acid
EFC	enzymatic fuel cell
EqB	equilibration buffer
F	phenylalanine (Phe)
H	histidine (His)
H_{AB}	coupling between electron donor and acceptor
His-tag	histidine-tag
IR	infrared
I_{SS}	steady-state current
k_{cat}	catalytic turnover rate
k_{ET}	electron transfer rate constant
K_M	Michaelis–Menten constant
L	leucine (Leu)
LMCT	ligand-to-metal charge transfer
M	methionine (Met)
MCO	multicopper oxidase
MD	molecular dynamics
MWBP	multiwalled CNT BP
MWBP-F	functionalized multiwalled CNT-BP
MWCNT	multiwalled CNT
MWCO	molecular weight cutoff
NMR	nuclear magnetic resonance
OCP	open circuit potential
OD	optical density
ORR	oxygen reduction reaction
PBSE	1-pyrenebutanoic acid, succinimidyl ester
PhB	phosphate buffer
p*Ka*	acid dissociation constant
RDE	rotating disc electrode
R_L	ratio of the high-energy state to the low-energy state

SLAC	small laccase from *Streptomyces coelicolor*
SWBP	single walled CNT BP
T	threonine (Thr)
T1	type 1 Copper
T2/T3	type 2/Type 3 copper
UV–Vis	ultraviolet–visible
V	valine (Val)
WT	wild type
Y	tyrosine (Tyr)